

Understanding large-scale dynamos in unstratified rotating shear flows

Tushar Mondal,^{1,*} Pallavi Bhat,^{1,†} Fatima Ebrahimi,^{2,3,‡} and Eric G. Blackman^{4,§}

¹*International Centre for Theoretical Sciences, Tata Institute of Fundamental Research, Bengaluru 560089, India*

²*Princeton Plasma Physics Laboratory, Princeton University, Princeton, NJ 08543, USA*

³*Department of Astrophysical Sciences, Princeton University, Princeton, NJ 08544, USA*

⁴*Department of Physics and Astronomy, University of Rochester, Rochester, NY 14627, USA*

We combine simulations with new analyses that overcome previous pitfalls to explicate how non-helical mean-field dynamos grow and saturate in unstratified, magnetorotationally driven turbulence. Shear of the mean radial magnetic field amplifies the azimuthal component. Radial fields are regenerated by velocity fluctuations that induce shear of radial magnetic fluctuations, followed by Lorentz and Coriolis forces that source a negative off-diagonal component in the turbulent diffusivity tensor. We present a simple schematic to illustrate this dynamo growth. A different part of the Lorentz force forms a third-order correlator in the mean electromotive force that saturates the dynamo.

Rotating shear flows are common in astrophysical accretion disks that drive phenomena such as planet formation, X-ray binaries and jets in protostars and compact objects. The disks are unstable to the magnetorotational instability (MRI), which drives turbulence that facilitates outward angular momentum transport [1]. While MRI turbulence requires sufficiently coherent magnetic fields for sustenance [2], it simultaneously dissipates them via turbulent diffusion. Numerical simulations of MRI turbulence have consistently revealed the prevalence and importance of large-scale magnetic dynamos in characterizing and sustaining the steady-state [3–8]. In mean-field dynamo theory [9–12], the evolution of the large-scale magnetic field is governed by:

$$\frac{\partial \bar{\mathbf{B}}}{\partial t} = \nabla \times (\bar{\mathbf{U}} \times \bar{\mathbf{B}} + \bar{\mathcal{E}} - \eta \mu_0 \bar{\mathbf{J}}), \quad (1)$$

where $\bar{\mathbf{U}}$, $\bar{\mathbf{B}}$, and $\bar{\mathbf{J}}$ represent the large-scale (mean) velocity, magnetic field, and current density, respectively. The mean electromotive force (EMF), $\bar{\mathcal{E}} = \overline{\mathbf{u} \times \mathbf{b}}$, encapsulates the correlation between fluctuating velocity and magnetic fields. In traditional mean-field closure, the EMF is modeled as $\bar{\mathcal{E}}_i = \alpha_{ij} \bar{B}_j + \beta_{ijk} \bar{B}_{j,k} = \alpha_{ij} \bar{B}_j - \eta_{ij} \bar{J}_j$, where α_{ij} and η_{ij} (or β_{ijk}) are turbulent transport coefficients determined by small-scale dynamics.

Determining the physical origin of the coefficients in this formalism that best capture large-scale MRI growth in simulations has been an active area of research. Several theoretical investigations, including studies of nonlinear mode coupling in the subcritical nature of the MRI dynamo [13–15], nonlinear transverse cascades [16, 17], the role of turbulent resistivity on the self-regulation of MRI turbulence [18, 19], and minimal ingredients required for large-scale field growth from quasi-linear analysis [20–22], have been conducted to better understand MRI turbulence and associated dynamo behavior.

In vertically stratified, differentially rotating disks, the traditional α – Ω dynamo possibly explains large-scale magnetic field generation: the α -effect, driven by helical turbulence, generates poloidal fields, while the Ω -effect, from differential rotation, shears them into toroidal fields [6, 23–25]. However, simulations of MRI turbulence in unstratified rotating shear flows exhibit predominantly non-helical, large-scale magnetic fields [7, 24, 26–28], raising fundamental questions about alternative dynamo mechanisms that do not rely on mean helicities.

A leading hypothesis attributes such non-helical large-scale dynamos to a negative off-diagonal component of the turbulent diffusivity tensor, arising from shear, rotation, or their combination. Rotation alone produces the $\mathbf{\Omega} \times \mathbf{J}$ (Rädler) effect [29], while shear may induce the (kinetic or magnetic) shear-current effect [30–32]. However, the role and reliability of these effects remain debated, as their interpretation is limited by closure approximations and difficulties in simultaneously extracting all turbulent transport coefficients amid strong fluctuations and oscillatory large-scale fields [33].

Another pressing question is how dynamos driven by negative η_{yx} saturate. Previous studies hypothesized that saturation occurs through a sign reversal of η_{yx} after the initial growth phase [34]. However, Ref. [24] showed that η_{yx} remains consistently negative throughout both the linear and nonlinear stages. A complete physical understanding of non-helical MRI large-scale dynamos and their saturation remains elusive.

To address these outstanding issues, we present a fundamentally new approach based on a self-consistent formulation of the mean EMF, whose mathematical framework was first introduced through direct statistical simulations (DSS) [8]. The EMF is constructed from the evolution equations of the Faraday tensor $\bar{F}_{ij} = \overline{u_i b_j}$, which contains interaction terms involving the Coriolis force and background shear—core features of rotating shear flows. These terms mediate couplings between different components of \bar{F}_{ij} , and by systematically analyzing these couplings, we derive exact expressions for the EMF and associated turbulent transport coefficients. The resulting EMF contains not only the familiar terms proportional to

* tushar.mondal@icts.res.in

† pallavi.bhat@icts.res.in

‡ ebrahimi@princeton.edu

§ blackman@pas.rochester.edu

\bar{B}_i and its gradients, as in traditional mean-field closures, but also contributions from gradients of \bar{U}_i , third-order correlators, and pressure fluctuations. In earlier DSS-based approaches, closure models were required for the third-order terms [8]. Here, we perform direct numerical simulations (DNS) using the PENCIL CODE [35] to compute each EMF contribution explicitly, avoiding any a priori closure. Unlike previous methods, our formulation yields explicit, self-consistent expressions without relying on fitting procedures or closure approximations. This enables us to unambiguously identify the dominant source term responsible for large-scale magnetic field generation. To uncover its physical origin, we further analyze the evolution equations of the relevant fluctuating fields that make up the correlators. We refer to the growth mechanism as the rotation-shear-current (RSC) effect. It operates via a negative turbulent diffusivity component, η_{yx} , which remains negative throughout both the linear and nonlinear stages.

Horizontal planar averaging, denoted by $\bar{\cdot}$ or $\langle \cdot \rangle$, defines the large-scale field in our investigation of large-scale dynamos in MRI turbulence. Here we adopt Cartesian coordinates (x, y, z) corresponding to the radial, azimuthal, and vertical directions of the disk, respectively. Fig. 1(a) shows the time evolution of magnetic energy densities (scaled by two) for large-scale (\bar{B}_i^2) and fluctuating ($\bar{M}_{ii} = \bar{b}_i^2$) components. Fluctuating fields are comparable to or even stronger than large-scale fields during the exponential growth phase, with the azimuthal component dominating at both scales throughout nonlinear saturation. To understand the origin and sustenance of these large-scale fields, we analyze the xy -averaged mean-field induction equations derived from Eq.(1):

$$\partial_t \bar{B}_x = -\partial_z \bar{\mathcal{E}}_y - \bar{U}_z \partial_z \bar{B}_x + \bar{B}_z \partial_z \bar{U}_x, \quad (2a)$$

$$\partial_t \bar{B}_y = -q\Omega \bar{B}_x + \partial_z \bar{\mathcal{E}}_x - \bar{U}_z \partial_z \bar{B}_y + \bar{B}_z \partial_z \bar{U}_y. \quad (2b)$$

Here, $-q\Omega \bar{B}_x$ is the shear term due to a linear background shear, $\mathbf{U}^0 = -q\Omega x \hat{y}$, with $q = 3/2$ for Keplerian disks. The terms $\bar{\mathbf{U}} \cdot \nabla \bar{\mathbf{B}}$ and $\bar{\mathbf{B}} \cdot \nabla \bar{\mathbf{U}}$ represent advection and stretching, respectively. The mean EMF components are $\bar{\mathcal{E}}_x = (\bar{F}_{yz} - \bar{F}_{zy})$ and $\bar{\mathcal{E}}_y = (\bar{F}_{zx} - \bar{F}_{xz})$. As established in Ref. [8], \bar{B}_x is generated by the vertical gradient of the azimuthal EMF, $\partial_z \bar{\mathcal{E}}_y$, while shear stretches \bar{B}_x into \bar{B}_y via the Ω -effect. In contrast, the vertical gradient of the radial EMF, $\partial_z \bar{\mathcal{E}}_x$, extracts energy from \bar{B}_y , acting as a sink. The key is to understand how $\bar{\mathcal{E}}_y$ drives the growth of \bar{B}_x in a self-sustaining dynamo.

The EMF can be constructed from the evolution equa-

tions of the Faraday tensors (see Appendix A):

$$\begin{aligned} \bar{\mathcal{E}}_y = & \frac{-1}{q(2-q)\Omega} \left[\left\{ -q\mathcal{D}_t \bar{F}_{yz} + (2-q)\mathcal{D}_t \bar{F}_{zy} \right\} \right. \\ & - 2\bar{F}_{zz} \partial_z \bar{U}_y + \frac{1}{\rho} \left\{ q\bar{M}_{zz} + (2-q)\bar{R}_{zz} \right\} \partial_z \bar{B}_y \\ & + \bar{B}_k \left\{ q \left(\langle u_y \partial_k u_z \rangle + \frac{\langle b_z \partial_k b_y \rangle}{\mu_0 \rho} \right) - (2-q) \right. \\ & \left. \times \left(\langle u_z \partial_k u_y \rangle + \frac{\langle b_y \partial_k b_z \rangle}{\mu_0 \rho} \right) \right\} \left. \right] + \bar{\mathcal{P}}_y + \bar{\mathcal{T}}_y. \quad (3) \end{aligned}$$

Here, $\mathcal{D}_t = \partial_t - q\Omega x \partial_y$ includes advection by the background shear. The third-order and pressure fluctuation terms are $\bar{\mathcal{T}}_y = -\{q\bar{\mathcal{T}}_{yz}^F - (2-q)\bar{\mathcal{T}}_{zy}^F\}/q(2-q)\Omega$, and $\bar{\mathcal{P}}_y = \{q\langle b_z \partial_y p_t \rangle - (2-q)\langle b_y \partial_z p_t \rangle\}/q(2-q)\rho\Omega$, where $\bar{\mathcal{T}}_{ij}^F = \langle u_i b_k \partial_k u_j + b_j b_k \partial_k b_i - u_k \partial_k F_{ij} \rangle$, and $p_t = p_g + p_b$ is the total (gas + magnetic) pressure fluctuation. The EMF $\bar{\mathcal{E}}_y$ consists of terms proportional to \bar{B}_i , its gradients, gradients of \bar{U}_i , third-order correlators, pressure fluctuations, and time derivatives of \bar{F}_{ij} . Substituting Eq. (3) into Eq. (2a), we obtain:

$$\begin{aligned} \partial_t \bar{B}_x = & -\partial_z \bar{\mathcal{E}}_y = -\partial_z \left[\alpha_{yj} \bar{B}_j + \beta_{yyz} \partial_z \bar{B}_y + \chi_{yyz} \partial_z \bar{U}_y \right. \\ & \left. + \bar{\mathcal{P}}_y + \bar{\mathcal{T}}_y + \mathcal{D}_t \langle \cdot \cdot \cdot \rangle \right], \quad (4) \end{aligned}$$

where α_{ij} , β_{ijk} , and χ_{ijk} are the turbulent transport coefficients, derived from Eq. (3). The off-diagonal turbulent diffusivity component is given by

$$\eta_{yx} = \beta_{yyz} = -\frac{1}{\rho\Omega} \left[\frac{1}{2-q} \bar{M}_{zz} + \frac{1}{q} \bar{R}_{zz} \right]. \quad (5)$$

For Keplerian shear ($q = 1.5$), η_{yx} remains negative because \bar{M}_{zz} and \bar{R}_{zz} —the energies associated with vertical magnetic and velocity fluctuations—are always positive, thereby driving the amplification of large-scale magnetic fields. The magnetic-shear-current (MSC) effect [34] also originates from a negative η_{yx} , but the RSC effect in Eq. (5) is fundamentally distinct from the MSC effect. In the MSC framework, a negative η_{yx} arises from magnetic fluctuations interacting with shear and a large-scale magnetic field gradient, with the pressure response of velocity fluctuations playing a central role. Rotation is not essential in this process, and the turbulence is maintained by external forcing. In contrast, in our simulations the turbulence is entirely MRI-driven, without external forcing, and is therefore intrinsically tied to rotation. We show later in this work that the Coriolis force plays a central role in coupling Lorentz-force-driven fluctuations to the EMF. In the absence of rotation, the magnetic term in Eq. (5) changes sign and becomes diffusive, so η_{yx} no longer guarantees a net dynamo effect. The overall sign may then depend on the energy spectra [33].

Figs. 1(b) and (c) show how each term in $\bar{\mathcal{E}}_y$ contributes to the generation of $\bar{B}_x(z)$ during two key MRI stages:

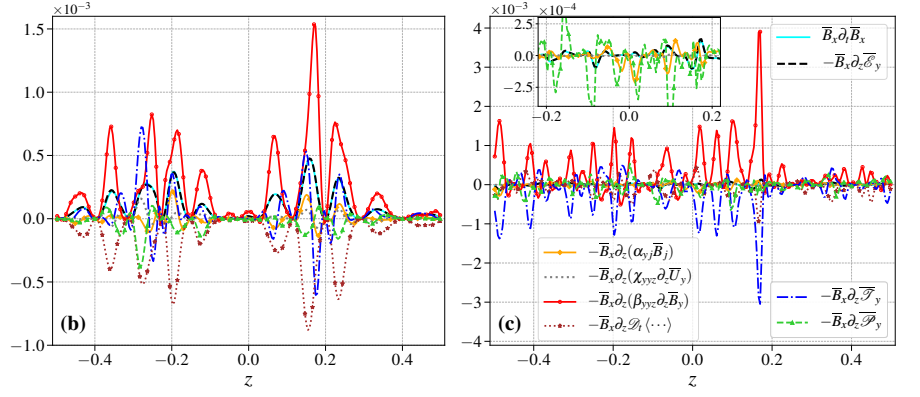
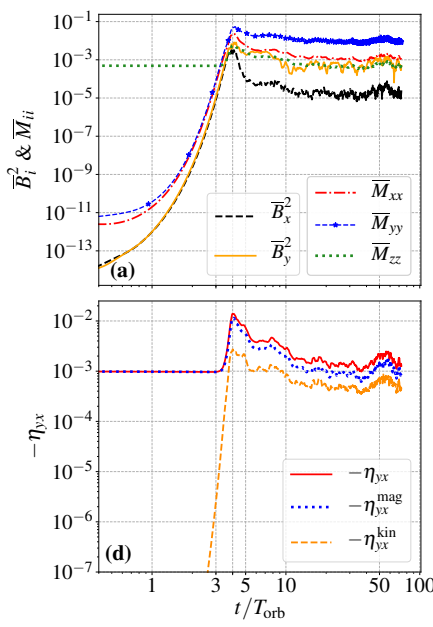


FIG. 1: (a) Time evolution of magnetic energy densities (scaled by two) for xy -averaged large-scale and fluctuating fields. (b), (c) Spatial variation of individual terms from the vertical gradient of $\bar{\mathcal{E}}_y$ (Eq. 4) responsible for generating $\bar{B}_x(z)$, shown during (b) exponential growth ($t/T_{orb} = 3.34$) and (c) nonlinear stage ($t/T_{orb} = 60$). Line styles and colors are consistent in (b) and (c); legend is shown in panel (c). (d) Time evolution of the off-diagonal turbulent diffusivity η_{yx} (Eq. 5). In (a) and (d), additional averaging along z is applied.

(b) the exponential growth phase at $t/T_{orb} = 3.34$, and (c) the nonlinear saturation stage at $t/T_{orb} = 60$. For clarity, we multiply \bar{B}_x on both sides of Eq. (4), ensuring the source term remains positive regardless of the sign of \bar{B}_x growth. During the exponential growth (Fig. 1b), the dominant source is the magnetic field gradient term (linked to β_{yyz} or η_{yx}), which amplifies $\bar{B}_x(z)$. The time-derivative term is predominantly dissipative, while terms proportional to \bar{B}_i and velocity gradients are negligible. The third-order correlator exhibits localized variations that can either enhance or counteract the mean-field growth. In the nonlinear stage (Fig. 1c), third-order correlators become dominant and counteract the η_{yx} -driven growth, sustaining dynamo self-regulation.

The large-scale dynamo mechanism, governed by $\eta_{yx}\bar{J}_x$ or $\beta_{yyz}\partial_z\bar{B}_y$, is known as the rotation-shear-current effect [8]. According to Eq. (5), the total off-diagonal diffusivity, $\eta_{yx} = \eta_{yx}^{\text{mag}} + \eta_{yx}^{\text{kin}}$, comprises a magnetic contribution (linked to M_{zz}) and a kinetic one (linked to \bar{R}_{zz}). The magnetic component dominates the dynamo, while the kinetic part remains subdominant throughout the evolution, as shown in Fig. 1(d). We now examine the physical origin of this mechanism, which operates through a negative η_{yx} , primarily its magnetic component η_{yx}^{mag} , in $\bar{\mathcal{E}}_y$. Specifically, we analyze how the term $\bar{M}_{zz}\partial_z\bar{B}_y$ contributes to $\bar{\mathcal{E}}_y$, thereby sustaining the mean field B_x .

In the presence of both mean ($\bar{J}_x = -\partial_z\bar{B}_y$) and fluctuating ($j_x = -\partial_z b_y$) currents, magnetic fluctuations b_z interact with these field gradients to drive velocity fluctuations u_y via the magnetic tension term $[(\mathbf{B} \cdot \nabla)B_y]_{\text{fluc}}$ in the fluctuating Lorentz force, particularly

$$u_y \sim \frac{\tau_y}{\mu_0 \rho} (b_z \partial_z \bar{B}_y + b_z \partial_z b_y). \quad (6)$$

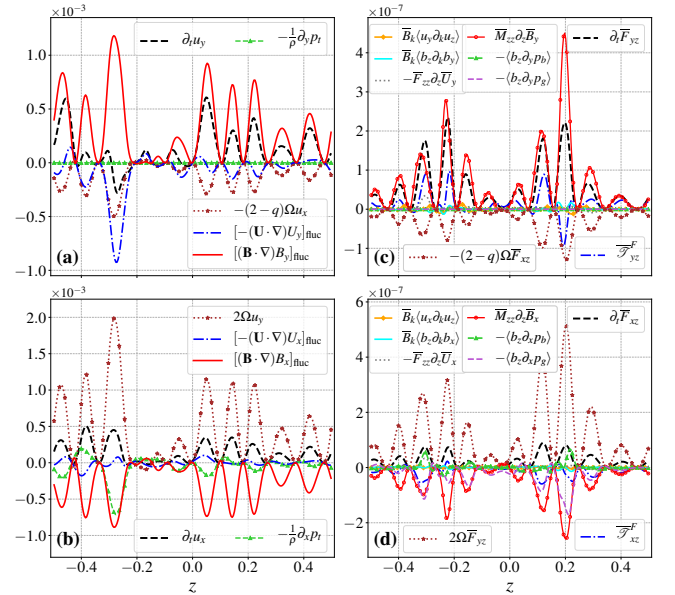


FIG. 2: Spatial variation of individual terms in the evolution equations for fluctuating velocity fields and mean Faraday stress during the MRI growth phase, evaluated at $t/T_{orb} = 3.34$. Panels (a, b) show terms for u_y and u_x (Eq. A1); panels (c, d) for \bar{F}_{yz} and \bar{F}_{xz} (Eq. A3). To ensure interpretability, we multiply u_i and \bar{F}_{ij} on both sides of their respective equations so that source terms remain positive (not shown in legends).

The Coriolis force subsequently converts u_y into u_x :

$$u_x \sim \tau_x 2\Omega u_y \sim 2\Omega \tau_x \frac{\tau_y}{\mu_0 \rho} (b_z \partial_z \bar{B}_y + b_z \partial_z b_y), \quad (7)$$

where, τ_i is the turbulent correlation time. Fig. 2 il-

illustrates the contribution of individual terms in the u_i evolution equations (see Appendix A). To track the energy we multiply u_i on both sides of the $\partial_t u_i$ equations. The magnetic tension term of Lorentz force fluctuations drives u_y (Fig. 2a), which is then converted into u_x by the Coriolis force (Fig. 2b). Contributions from pressure fluctuations are negligible for u_y , and remain small (mostly dissipative) in the u_x evolution.

The resulting u_x correlates with its source b_z , producing an EMF $\bar{\mathcal{E}}_y = \langle u_z b_x \rangle - \langle u_x b_z \rangle$, that is proportional to and has the same sign as \bar{J}_x :

$$\begin{aligned} \bar{\mathcal{E}}_y &\sim -\langle u_x b_z \rangle \sim -\tau_x 2\Omega \langle u_y b_z \rangle \\ &\sim -2\Omega \tau_x (\bar{M}_{zz} \partial_z \bar{B}_y + \langle b_z b_z \partial_z b_y \rangle) \\ &\sim 2\Omega \tau_x (\bar{M}_{zz} \bar{J}_x - \langle b_z b_z \partial_z b_y \rangle), \end{aligned} \quad (8)$$

where the second term on the RHS is a third-order correlator. Through its correlation with positive \bar{M}_{zz} , \bar{J}_x generates $\bar{\mathcal{E}}_y$, responsible for the growth of \bar{B}_x . This process underpins the origin of the negative η_{yx}^{mag} , through which the large-scale dynamo mechanism—rotation-shear-current effect—operates. Meanwhile, u_y correlates with b_z to produce $\bar{\mathcal{E}}_x = \langle u_y b_z \rangle - \langle u_z b_y \rangle$, which is proportional to but opposite in sign to \bar{J}_x :

$$\begin{aligned} \bar{\mathcal{E}}_x &\sim \langle u_y b_z \rangle \sim \tau_y (\bar{M}_{zz} \partial_z \bar{B}_y + \langle b_z b_z \partial_z b_y \rangle) \\ &\sim \tau_y (-\bar{M}_{zz} \bar{J}_x + \langle b_z b_z \partial_z b_y \rangle). \end{aligned} \quad (9)$$

Thus, $\bar{\mathcal{E}}_x$ acts as a turbulent dissipation mechanism for the mean field \bar{B}_y , counteracting its growth. Figs. 2(c) and (d) illustrate the contributions of individual terms in the evolution equations (see Appendix A) for $\bar{F}_{yz} = \langle u_y b_z \rangle$ and $\bar{F}_{xz} = \langle u_x b_z \rangle$, evaluated during the MRI exponential growth phase at $t/T_{\text{orb}} = 3.34$. The dominant source term for \bar{F}_{yz} is $\bar{M}_{zz} \partial_z \bar{B}_y$ (Fig. 2c), with the Coriolis force converting \bar{F}_{yz} into \bar{F}_{xz} (Fig. 2d). In both cases, terms proportional to \bar{B}_i are negligible. While azimuthal gas and magnetic pressure gradients do not contribute to \bar{F}_{yz} , a weak radial pressure gradient affects \bar{F}_{xz} .

To support the physical interpretation of the rotation-shear-current effect, we present visualizations of fluctuating velocity fields from DNS. Figure 3 shows streamlines of fluctuating velocities, illustrating how magnetic tension drives u_y , which is subsequently converted into u_x by the Coriolis force. In panel (a), (u_y, u_z) streamlines in the y - z plane at $x = 0.25$ are overlaid on a colormap of the magnetic tension term $b_z \partial_z B_y$ from the u_y equation. The streamlines, along the y -direction, closely follow regions of strong magnetic tension, confirming its role as the primary driver of u_y . Panel (b) shows (u_x, u_z) streamlines in the x - z plane at $y = 0.25$, with a colormap of the Coriolis term from the u_x equation. The alignment of streamlines with regions of strong Coriolis acceleration demonstrates the efficient conversion of u_y into u_x .

To connect fluctuating fields to the mean EMF, Fig. 4 shows the relevant fluctuating fields and their correlator. Panel (a) displays the fluctuating velocity u_x ; panel (b), the fluctuating magnetic field b_z , and panel (c), their

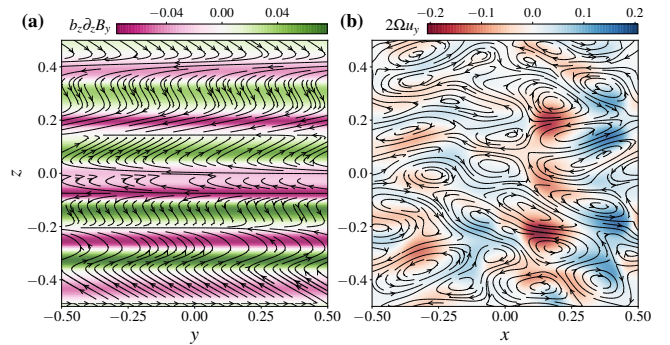


FIG. 3: Streamlines of in-plane fluctuating velocity fields during the exponential growth phase of MRI at $t/T_{\text{orb}} = 3.34$. (a) Streamlines of (u_y, u_z) in the y - z plane at $x = 0.25$, overlaid on a colormap of the magnetic tension term $b_z \partial_z B_y$, which drives u_y . (b) Streamlines of (u_x, u_z) in the x - z plane at $y = 0.25$, with a colormap of the Coriolis term, which converts u_y into u_x .

product $u_x b_z$, which contributes to the EMF component $\bar{\mathcal{E}}_y$. Although u_x and b_z individually average out when integrated over x —being nearly independent of y during the exponential growth phase—their product remains finite and structured, revealing a coherent correlation that sustains a nonzero EMF, $\bar{\mathcal{E}}_y(z) \sim -\langle u_x b_z \rangle$. This EMF is proportional to, and shares the sign of \bar{J}_x , reinforcing the generation of the mean field \bar{B}_x discussed earlier.

Finally, the mechanism underlying the rotation-shear-current effect is illustrated schematically in Fig. 5. Initially (panel a), two oppositely directed vertical magnetic field sectors are placed side by side (see Supplemental Material S1 for simulation setup). A small perturbation with a phase shift in x is introduced (panel b). Background shear ($\partial U_y^0 / \partial x < 0$) stretches the field lines and displaces the two sectors relative to each other (panel c). The bending of field lines induces radial currents $J_x \sim -\partial_z B_y$. The associated field curvature produces a magnetic tension force that drives velocity fluctuations u_y , which are subsequently redirected into u_x by the Coriolis force (panel d). These fluctuations produce an EMF component $\mathcal{E}_y \sim -u_x b_z$ (panel e). Notably, $\bar{\mathcal{E}}_y$ aligns coherently within each x - y plane but alternates in sign across z -layers. This results in a layerwise alternating EMF profile, $\bar{\mathcal{E}}_y(z)$, which drives the growth of a large-scale magnetic field $\bar{B}_x(z)$ (following Eq. 4) that reverses in z , consistent with the fastest-growing MRI mode.

In summary, we have demonstrated that, unlike traditional α - Ω dynamos that rely on helicity and stratification, large-scale dynamos in unstratified, zero-net-flux MRI-unstable disks arise through a fundamentally different mechanism—the rotation-shear-current effect. This dynamo operates through a negative off-diagonal turbulent diffusivity, η_{yx} , which amplifies large-scale radial magnetic fields. Horizontal planar averaging reveals that $\bar{\mathcal{E}}_y$ drives the generation of \bar{B}_x , which is then stretched into \bar{B}_y by shear via the Ω -effect, completing the dynamo

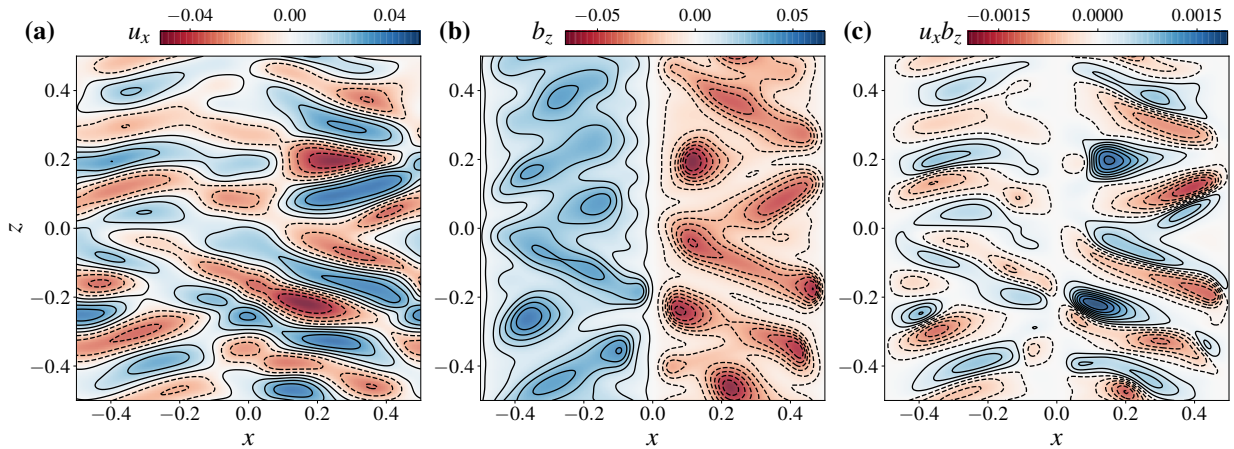


FIG. 4: Colormaps with contours of fluctuating fields in the x - z plane during the exponential growth phase of MRI, at $t/T_{\text{orb}} = 3.34$. (a) Fluctuating velocity u_x , (b) fluctuating magnetic field b_z , and (c) their product $u_x b_z$, with solid (dashed) contours denoting positive (negative) values. While fluctuations u_x and b_z individually average out when integrated over x , their correlator $u_x b_z$ remains finite, indicating a nonzero mean stress.

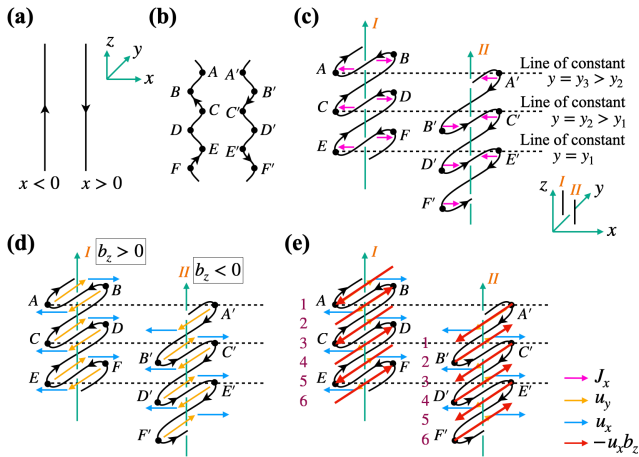


FIG. 5: Schematic illustration of the rotation-shear-current effect. (a) Two initially vertical magnetic field sectors with opposite polarity. (b) An x -dependent perturbation with a phase shift is introduced. (c) Background shear ($\partial U_y^0/\partial x < 0$) stretches the field lines and shifts the sectors relative to each other. The resulting field line bending produces radial currents $J_x \sim -\partial_z B_y$. (d) Magnetic tension from field curvature induces u_y fluctuations, which are converted into u_x via the Coriolis force. (e) The resulting vectors of $-u_x b_z$ are shown, with z -layers (1 to 6) indicating matched heights across stacks. The EMF component $\mathcal{E}_y \sim -u_x b_z$ aligns within each x - y plane at fixed z , but reverses sign between adjacent z -layers. After xy -averaging, $\bar{\mathcal{E}}_y(z)$ exhibits an alternating pattern: $\bar{\mathcal{E}}_y < 0$ at layer 1, $\bar{\mathcal{E}}_y > 0$ at layer 2, $\bar{\mathcal{E}}_y < 0$ at layer 3, and so on. The induced mean-field satisfies $\partial_t \bar{B}_x = -\partial_z \bar{\mathcal{E}}_y$, generating a coherent $\bar{B}_x(z)$ that reverses in z , consistent with the fastest-growing MRI mode.

cycle. The dominant source of $\bar{\mathcal{E}}_y$ is the magnetic contribution to turbulent diffusivity, η_{yx}^{mag} , arising from the interplay between fluctuating Lorentz and Coriolis forces. Specifically, magnetic tension $b_z \partial_z \bar{B}_y$ drives u_y via interactions between vertical magnetic fluctuations b_z and the mean current \bar{J}_x . The Coriolis force then converts u_y into u_x , which in turn correlates with b_z to produce an EMF $\mathcal{E}_y \sim -\langle u_x b_z \rangle$. This EMF is proportional to and has the same sign as \bar{J}_x , reinforcing the growth of \bar{B}_x and sustaining the dynamo. After the initial exponential growth, third-order correlators arising from Lorentz force fluctuations counteract the η_{yx} -driven amplification, saturating the dynamo in fully developed MRI turbulence.

Crucially, this work introduces a fundamentally new approach by constructing the mean EMF self-consistently from the evolution equations of Faraday tensors, enabling explicit identification of turbulent transport coefficients without any closure approximations or fitting procedures. By directly analyzing the evolution of fluctuating fields that constitute the EMF correlators, we uncover the complete production chain underlying large-scale magnetic field generation in MRI turbulence. This framework establishes a physically grounded method for diagnosing dynamo mechanisms in rotating shear flows as well as in global models with curvature effects [36, 37].

Acknowledgments:

The simulations were performed on the International Centre for Theoretical Sciences (ICTS) HPC cluster *Contra*. T.M. and P.B. acknowledge support of the Department of Atomic Energy, Government of India, under project no. RTI4001. E.B. acknowledges support from National Science Foundation (NSF) Physics Frontier Center grant PHY-2020249. F.E. acknowledges support from NSF under Award No. 2308839.

Appendix A: The Electromotive Force

In this section, we provide a comprehensive derivation of the electromotive force (EMF). Following standard mean-field theory, we apply a Reynolds decomposition to the dynamical flow variables, expressing each as the sum of a mean component (denoted by over-bars) and a fluctuating component (represented by lowercase letters): $B_i = \bar{B}_i + b_i$. This decomposition satisfies Reynolds averaging rules, i.e., $\bar{b}_i = 0$, $\bar{\bar{B}}_i = \bar{B}_i$. By subtracting the mean (in this case, the xy-averaged) equation from the total, we obtain the evolution equations for the fluctuating velocity and magnetic fields:

$$\begin{aligned} \mathcal{D}_t u_i &= q\Omega u_x \hat{y} - 2\epsilon_{ijk}\Omega_j u_k - [(\mathbf{U} \cdot \nabla)U_i]_{\text{fluc}} + \frac{1}{\mu_0\rho} [(\mathbf{B} \cdot \nabla)B_i]_{\text{fluc}} - \frac{1}{\rho} \partial_i p_t + \nu \partial_{jj} u_i \\ &= q\Omega u_x \hat{y} - 2\epsilon_{ijk}\Omega_j u_k - \bar{U}_j \partial_j u_i - u_j \partial_j \bar{U}_i + \frac{1}{\mu_0\rho} (\bar{B}_j \partial_j b_i + b_j \partial_j \bar{B}_i) + \frac{1}{\rho} \partial_j (M_{ij} - R_{ij} - \bar{M}_{ij} + \bar{R}_{ij}) \\ &\quad - \frac{1}{\rho} \partial_i p_t + \nu \partial_{jj} u_i, \end{aligned} \quad (\text{A1})$$

$$\mathcal{D}_t b_i = -q\Omega b_x \hat{y} + \bar{B}_j \partial_j u_i + b_j \partial_j \bar{U}_i - \bar{U}_j \partial_j b_i - u_j \partial_j \bar{B}_i + \partial_j (F_{ij} - F_{ji} - \bar{F}_{ij} + \bar{F}_{ji}) + \eta \partial_{jj} b_i. \quad (\text{A2})$$

Here, $\mathcal{D}_t = \partial_t - q\Omega x \partial_y$ includes advection by the background shear. $M_{ij} = b_i b_j / \mu_0$, $R_{ij} = \rho u_i u_j$, and $F_{ij} = u_i b_j$ represent the Maxwell, Reynolds, and Faraday tensors, respectively. Using Eqs. (A1) and (A2), and by applying Reynolds averaging rules, we obtain the evolution equation for the mean Faraday tensors:

$$\begin{aligned} \mathcal{D}_t \bar{F}_{ij} + \bar{U}_k \partial_k \bar{F}_{ij} - \bar{F}_{ik} \partial_k \bar{U}_j + \bar{F}_{kj} \partial_k \bar{U}_i + 2\epsilon_{ikl}\Omega_k \bar{F}_{lj} + \bar{S}_{ij}^F - \frac{1}{\rho} (\bar{M}_{jk} \partial_k \bar{B}_i - \bar{R}_{ik} \partial_k \bar{B}_j) \\ = -\frac{1}{\rho} \langle b_j \partial_i p_t \rangle + \bar{B}_k \langle u_i \partial_k u_j \rangle + \frac{\bar{B}_k}{\mu_0\rho} \langle b_j \partial_k b_i \rangle + \bar{T}_{ij}^F + \eta \langle u_i \partial_k b_j \rangle + \nu \langle b_j \partial_k u_i \rangle. \end{aligned} \quad (\text{A3})$$

Here, $\bar{S}_{ij}^F = -\bar{F}_{ik} \partial_k \bar{U}_j^0 + \bar{F}_{kj} \partial_k \bar{U}_i^0$ describes how the Faraday tensors are ‘stretched’ by the background shear flow, \mathbf{U}^0 , while $\bar{T}_{ij}^F = \langle u_i b_k \partial_k u_j + b_j b_k \partial_k b_i - u_k \partial_k F_{ij} \rangle$ represents the nonlinear third-order correlator. To construct the EMF, we utilize interaction terms from the Coriolis force and background shear in the evolution equations for the Faraday tensors. Our primary focus is on the azimuthal component of the EMF, given by: $\bar{\mathcal{E}}_y = \bar{F}_{zx} - \bar{F}_{xz}$. The evolution equations for the relevant Faraday tensor components are:

$$\begin{aligned} \mathcal{D}_t \bar{F}_{yz} &= -(2-q)\Omega \bar{F}_{xz} - \frac{1}{\rho} \langle b_z \partial_y p_t \rangle + (\bar{F}_{yk} \partial_k \bar{U}_z - \bar{F}_{kz} \partial_k \bar{U}_y) + \bar{B}_k \left[\langle u_y \partial_k u_z \rangle + \frac{\langle b_z \partial_k b_y \rangle}{\mu_0\rho} \right] \\ &\quad + \frac{1}{\rho} (\bar{M}_{zk} \partial_k \bar{B}_y - \bar{R}_{yk} \partial_k \bar{B}_z) + \bar{T}_{yz}^F, \end{aligned} \quad (\text{A4})$$

$$\begin{aligned} \mathcal{D}_t \bar{F}_{zy} &= -q\Omega \bar{F}_{zx} - \frac{1}{\rho} \langle b_y \partial_z p_t \rangle + (\bar{F}_{zk} \partial_k \bar{U}_y - \bar{F}_{ky} \partial_k \bar{U}_z) + \bar{B}_k \left[\langle u_z \partial_k u_y \rangle + \frac{\langle b_y \partial_k b_z \rangle}{\mu_0\rho} \right] \\ &\quad + \frac{1}{\rho} (\bar{M}_{yk} \partial_k \bar{B}_z - \bar{R}_{zk} \partial_k \bar{B}_y) + \bar{T}_{zy}^F. \end{aligned} \quad (\text{A5})$$

To derive $\bar{\mathcal{E}}_y$, we multiply Eq. (A4) by q and Eq. (A5) by $(q-2)$, and subsequently combine them. After algebraic simplifications, we obtain:

$$\begin{aligned} q\mathcal{D}_t \bar{F}_{yz} + (q-2)\mathcal{D}_t \bar{F}_{zy} &= q(2-q)\Omega (\bar{F}_{zx} - \bar{F}_{xz}) + \{q\bar{F}_{yk} + (2-q)\bar{F}_{ky}\} \partial_k \bar{U}_z - \{q\bar{F}_{kz} + (2-q)\bar{F}_{zk}\} \partial_k \bar{U}_y \\ &\quad + \frac{1}{\rho} \{q\bar{M}_{zk} + (2-q)\bar{R}_{zk}\} \partial_k \bar{B}_y - \frac{1}{\rho} \{q\bar{R}_{yk} + (2-q)\bar{M}_{yk}\} \partial_k \bar{B}_z \\ &\quad + \bar{B}_k \left\{ q \left(\langle u_y \partial_k u_z \rangle + \frac{\langle b_z \partial_k b_y \rangle}{\mu_0\rho} \right) - (2-q) \left(\langle u_z \partial_k u_y \rangle + \frac{\langle b_y \partial_k b_z \rangle}{\mu_0\rho} \right) \right\} \\ &\quad - \frac{1}{\rho} \left\{ q \langle b_z \partial_y p_t \rangle - (2-q) \langle b_y \partial_z p_t \rangle \right\} + \bar{T}_y, \end{aligned} \quad (\text{A6})$$

where, $\bar{\mathcal{T}}_y = q\bar{\mathcal{T}}_{yz}^F - (2-q)\bar{\mathcal{T}}_{zy}^F$ represents the contribution from third-order correlators. By further algebraic manipulation, we arrive at the final expression for $\bar{\mathcal{E}}_y = (\bar{F}_{zx} - \bar{F}_{xz})$:

$$\begin{aligned} \bar{\mathcal{E}}_y = \frac{-1}{q(2-q)\Omega} \left[\right. & \left\{ -q\mathcal{D}_t\bar{F}_{yz} + (2-q)\mathcal{D}_t\bar{F}_{zy} \right\} + \left\{ q\bar{F}_{yk} + (2-q)\bar{F}_{ky} \right\} \partial_k\bar{U}_z - \left\{ q\bar{F}_{kz} + (2-q)\bar{F}_{zk} \right\} \partial_k\bar{U}_y \\ & + \frac{1}{\rho} \left\{ q\bar{M}_{zk} + (2-q)\bar{R}_{zk} \right\} \partial_k\bar{B}_y - \frac{1}{\rho} \left\{ q\bar{R}_{yk} + (2-q)\bar{M}_{yk} \right\} \partial_k\bar{B}_z \\ & + \bar{B}_k \left\{ q \left(\langle u_y \partial_k u_z \rangle + \frac{\langle b_z \partial_k b_y \rangle}{\mu_0 \rho} \right) - (2-q) \left(\langle u_z \partial_k u_y \rangle + \frac{\langle b_y \partial_k b_z \rangle}{\mu_0 \rho} \right) \right\} \\ & \left. - \frac{1}{\rho} \left\{ q \langle b_z \partial_y p_t \rangle - (2-q) \langle b_y \partial_z p_t \rangle + \bar{\mathcal{T}}_y \right\} \right]. \end{aligned} \quad (\text{A7})$$

-
- [1] S. A. Balbus and J. F. Hawley, Instability, turbulence, and enhanced transport in accretion disks, *Reviews of Modern Physics* **70**, 1 (1998).
- [2] P. Bhat, F. Ebrahimi, E. G. Blackman, and K. Subramanian, Evolution of the magnetorotational instability on initially tangled magnetic fields, *Mon. Not. R. Astron. Soc.* **472**, 2569 (2017).
- [3] A. Brandenburg, A. Nordlund, R. F. Stein, and U. Torkelsson, Dynamo-generated Turbulence and Large-Scale Magnetic Fields in a Keplerian Shear Flow, *Astrophys. J.* **446**, 741 (1995).
- [4] J. F. Hawley, C. F. Gammie, and S. A. Balbus, Local Three-dimensional Simulations of an Accretion Disk Hydromagnetic Dynamo, *Astrophys. J.* **464**, 690 (1996).
- [5] G. Lesur and G. I. Ogilvie, On self-sustained dynamo cycles in accretion discs, *Astron. Astrophys.* **488**, 451 (2008).
- [6] O. Gressel, A mean-field approach to the propagation of field patterns in stratified magnetorotational turbulence, *Mon. Not. R. Astron. Soc.* **405**, 41 (2010).
- [7] P. Bhat, F. Ebrahimi, and E. G. Blackman, Large-scale dynamo action precedes turbulence in shearing box simulations of the magnetorotational instability, *Mon. Not. R. Astron. Soc.* **462**, 818 (2016).
- [8] T. Mondal and P. Bhat, Unified treatment of mean-field dynamo and angular-momentum transport in magnetorotational instability-driven turbulence, *Phys. Rev. E* **108**, 065201 (2023).
- [9] F. Krause and K. H. Raedler, *Mean-field magnetohydrodynamics and dynamo theory* (Pergamon Press, Oxford, 1980).
- [10] A. Brandenburg and K. Subramanian, Astrophysical magnetic fields and nonlinear dynamo theory, *Phys. Rep.* **417**, 1 (2005).
- [11] F. Rincon, Dynamo theories, *Journal of Plasma Physics* **85**, 205850401 (2019).
- [12] S. M. Tobias, The turbulent dynamo, *Journal of Fluid Mechanics* **912**, P1 (2021).
- [13] F. Rincon, G. I. Ogilvie, and M. R. E. Proctor, Self-Sustaining Nonlinear Dynamo Process in Keplerian Shear Flows, *Phys. Rev. Lett.* **98**, 254502 (2007).
- [14] J. Hecault, F. Rincon, C. Cossu, G. Lesur, G. I. Ogilvie, and P. Y. Longaretti, Periodic magnetorotational dynamo action as a prototype of nonlinear magnetic-field generation in shear flows, *Phys. Rev. E* **84**, 036321 (2011).
- [15] A. Riols, F. Rincon, C. Cossu, G. Lesur, G. I. Ogilvie, and P. Y. Longaretti, Magnetorotational dynamo chimeras. The missing link to turbulent accretion disk dynamo models?, *Astron. Astrophys.* **598**, A87 (2017).
- [16] G. Mamatsashvili, G. Chagelishvili, M. E. Pessah, F. Stefani, and G. Bodo, Zero Net Flux MRI Turbulence in Disks: Sustainance Scheme and Magnetic Prandtl Number Dependence, *Astrophys. J.* **904**, 47 (2020).
- [17] L. E. Held, G. Mamatsashvili, and M. E. Pessah, MRI turbulence in vertically stratified accretion discs at large magnetic Prandtl numbers, *Mon. Not. R. Astron. Soc.* **530**, 2232 (2024).
- [18] M. C. Begelman and P. J. Armitage, Saturation of the magnetorotational instability and the origin of magnetically elevated accretion discs, *Mon. Not. R. Astron. Soc.* **521**, 5952 (2023).
- [19] M. C. Begelman, A simple model of globally magnetized accretion discs, *Mon. Not. R. Astron. Soc.* **534**, 3144 (2024).
- [20] F. Ebrahimi, S. C. Prager, and D. D. Schnack, Saturation of Magnetorotational Instability Through Magnetic Field Generation, *Astrophys. J.* **698**, 233 (2009).
- [21] T. Heinemann, J. C. McWilliams, and A. A. Schekochihin, Large-Scale Magnetic Field Generation by Randomly Forced Shearing Waves, *Phys. Rev. Lett.* **107**, 255004 (2011).
- [22] F. Ebrahimi and E. G. Blackman, Radially dependent large-scale dynamos in global cylindrical shear flows and the local cartesian limit, *Mon. Not. R. Astron. Soc.* **459**, 1422 (2016).
- [23] O. Gressel and M. E. Pessah, Characterizing the Mean-field Dynamo in Turbulent Accretion Disks, *Astrophys. J.* **810**, 59 (2015).
- [24] J.-M. Shi, J. M. Stone, and C. X. Huang, Saturation of the magnetorotational instability in the unstratified shearing box with zero net flux: convergence in taller boxes, *Mon. Not. R. Astron. Soc.* **456**, 2273 (2016).
- [25] P. Dhang, A. B. Bendre, and K. Subramanian, Shedding light on the MRI-driven dynamo in a stratified shearing box, *Mon. Not. R. Astron. Soc.* **530**, 2778 (2024).

- [26] R. Wissing, S. Shen, J. Wadsley, and T. Quinn, Magnetorotational instability with smoothed particle hydrodynamics, *Astron. Astrophys.* **659**, A91 (2022).
- [27] O. Zier and V. Springel, Simulating the magnetorotational instability on a moving mesh with the shearing box approximation, *Mon. Not. R. Astron. Soc.* **517**, 2639 (2022).
- [28] V. Skoutnev, J. Squire, and A. Bhattacharjee, On large-scale dynamos with stable stratification and the application to stellar radiative zones, *Mon. Not. R. Astron. Soc.* **517**, 526 (2022).
- [29] K. H. Rädler, Investigations of spherical kinematic mean-field dynamo models, *Astronomische Nachrichten* **307**, 89 (1986).
- [30] I. Rogachevskii and N. Kleeorin, Electromotive force and large-scale magnetic dynamo in a turbulent flow with a mean shear, *Phys. Rev. E* **68**, 036301 (2003).
- [31] I. Rogachevskii and N. Kleeorin, Nonlinear theory of a “shear-current” effect and mean-field magnetic dynamos, *Phys. Rev. E* **70**, 046310 (2004).
- [32] J. Squire and A. Bhattacharjee, Generation of Large-Scale Magnetic Fields by Small-Scale Dynamo in Shear Flows, *Phys. Rev. Lett.* **115**, 175003 (2015).
- [33] H. Zhou and E. G. Blackman, On the shear-current effect: toward understanding why theories and simulations have mutually and separately conflicted, *Mon. Not. R. Astron. Soc.* **507**, 5732 (2021).
- [34] J. Squire and A. Bhattacharjee, The magnetic shear-current effect: generation of large-scale magnetic fields by the small-scale dynamo, *Journal of Plasma Physics* **82**, 535820201 (2016).
- [35] A. Brandenburg et al. (Pencil Code Collaboration), The Pencil Code, a modular MPI code for partial differential equations and particles: multipurpose and multiuser-maintained, *Journal of Open Source Software* **6**, 2807 (2021).
- [36] F. Ebrahimi and M. Pharr, A Nonlocal Magnetocurvature Instability in a Differentially Rotating Disk, *Astrophys. J.* **936**, 145 (2022).
- [37] F. Ebrahimi and A. Haywood, A generalized effective potential for differentially rotating plasmas, *Physics of Plasmas* **32**, 030702 (2025).
- [38] A. Brandenburg and D. Sokoloff, Local and Nonlocal Magnetic Diffusion and Alpha-Effect Tensors in Shear Flow Turbulence, *Geophysical and Astrophysical Fluid Dynamics* **96**, 319 (2002).

Supplemental Material

S1: Numerical Setup

This study employs direct numerical simulations (DNS) of unstratified, zero-net-magnetic-flux MRI turbulence in a Keplerian accretion disk. We adopt a Cartesian shearing-sheet approximation, where differential rotation is locally represented as a linear shear flow, $\mathbf{U}^0 = -q\Omega x\hat{y}$, with a uniform rotation rate, $\boldsymbol{\Omega} = \Omega\hat{z}$, and a shear parameter of $q = 3/2$. Here, x , y , and z correspond to the radial, azimuthal, and vertical directions, respectively. The system evolves according to the standard magnetohydrodynamic (MHD) equations in the rotating shearing frame:

$$\frac{\mathcal{D}\mathbf{A}}{\mathcal{D}t} = q\Omega A_y \hat{x} + \mathbf{U} \times \mathbf{B} - \eta\mu_0 \mathbf{J}, \quad (\text{S1})$$

$$\begin{aligned} \frac{\mathcal{D}\mathbf{U}}{\mathcal{D}t} = & -(\mathbf{U} \cdot \nabla)\mathbf{U} + q\Omega U_x \hat{y} - \frac{1}{\rho} \nabla P_g + \frac{1}{\rho} \mathbf{J} \times \mathbf{B} \\ & - 2\boldsymbol{\Omega} \times \mathbf{U} + \frac{1}{\rho} \nabla \cdot 2\nu\rho\mathbf{S}, \end{aligned} \quad (\text{S2})$$

$$\frac{\mathcal{D}\ln\rho}{\mathcal{D}t} = -(\mathbf{U} \cdot \nabla)\ln\rho - \nabla \cdot \mathbf{U}, \quad (\text{S3})$$

where \mathbf{U} is the velocity field, ρ the density, P_g the thermal pressure, η the magnetic diffusivity, and ν the microscopic viscosity. Here, $\mathcal{D}/\mathcal{D}t = \partial/\partial t - q\Omega x\partial_y$ includes advection by the background shear. The rate-of-strain tensor is defined as $\mathbf{S}_{ij} = \frac{1}{2}(\mathbf{U}_{i,j} + \mathbf{U}_{j,i} - \frac{2}{3}\delta_{ij}\nabla \cdot \mathbf{U})$. We assume an isothermal equation of state, $P_g = \rho c_s^2$, with constant sound speed c_s . We solve Eqs. (S1)–(S3) using the PENCIL CODE [35], a high-order finite-difference solver with sixth-order spatial accuracy and third-order time integration. The solenoidal constraint $\nabla \cdot \mathbf{B} = 0$ is enforced by evolving the magnetic vector potential \mathbf{A} , where $\mathbf{B} = \nabla \times \mathbf{A}$.

The computational domain is a cubic box spanning $-L_x/2 \leq x \leq L_x/2$, $-L_y/2 \leq y \leq L_y/2$, and $-L_z/2 \leq z \leq L_z/2$, with a uniform grid resolution of 256^3 . We impose periodic boundary conditions in the y (azimuthal) and z (vertical) directions, and shear-periodic conditions in the x (radial) direction. All quantities are normalized such that length is scaled by box size L , velocity by c_s , density by its initial value ρ_0 , and magnetic field by $(\mu_0\rho_0 c_s^2)^{1/2}$, where we set $L = \Omega = \rho_0 = \mu_0 = c_s = 1$.

The initial velocity field is Gaussian random noise with an amplitude of $10^{-4}c_s$. The initial zero-net-flux vertical magnetic field is set as $\mathbf{B} = B_0 \sin(k_x x)\hat{z}$, corresponding to a vector potential $\mathbf{A} = A_0 \cos(k_x x)\hat{y}$, with $A_0 = 0.005$ and $k_x = 2\pi/L_x$. The plasma beta parameter is $\beta = 2\mu_0 P_g / \bar{B}_0^2 \simeq 1014$. From linear MRI analysis, the wavenumber of maximum growth is $k_{\max}/k_1 = \sqrt{15/16}(\Omega/v_{A,0})/k_1 \approx 5$, where $v_{A,0} = B_0/\sqrt{\mu_0\rho_0}$ is the initial Alfvén speed, and $k_1 = 2\pi/L$. MRI-driven turbulence reaches a statistical steady state, with a root mean square (rms) velocity of $U_{\text{rms}} \sim 0.1c_s$, indicating weak compressibility. The fluid and magnetic Reynolds num-

bers are defined as $\text{Re} \equiv U_{\text{rms}}L/\nu$ and $\text{Rm} \equiv U_{\text{rms}}L/\eta$. For our DNS runs, we set $\nu = 8 \times 10^{-5}$ and $\eta = 2 \times 10^{-5}$, yielding $\text{Rm} \simeq 5000$ and a magnetic Prandtl number of $\text{Pm} \equiv \text{Rm}/\text{Re} = 4$.

To confirm robustness, we perform additional simulations: (i) at $\text{Pm} = 8$ ($\nu = 1.6 \times 10^{-4}$, $\eta = 2 \times 10^{-5}$) in a cubic domain with resolution 256^3 , and (ii) in a vertically elongated box with aspect ratio $L_x : L_y : L_z = 1 : 1 : 8$ and resolution $128 \times 128 \times 1024$ at $\text{Pm} = 8$ ($\nu = 3.2 \times 10^{-4}$, $\eta = 4 \times 10^{-5}$). Both cases yield consistent nonhelical dynamo behavior, supporting the robustness of our conclusions. Unless otherwise stated, results in the main text correspond to the $\text{Pm} = 4$ cubic box.

For the evaluation of turbulent correlations, we first compute horizontal planar averages to define the mean fields. Fluctuations are then obtained by subtracting these mean fields from the total fields and used to construct the relevant correlators. A second planar average is finally applied to obtain the EMF, stress tensors, and third-order correlators.

Linear MRI Dynamo Growth Rate: In the early, linear phase of the MRI, the evolution of the horizontally averaged mean magnetic field can be approximated by retaining only the dominant source term associated with the negative off-diagonal resistivity, $-\eta_{yx}$. All other terms (in Eq. 4) that act as sinks of magnetic energy are collectively modeled as a single effective diagonal turbulent resistivity, denoted by η_t . Assuming a mean-field mode with vertical structure $\propto \exp(\gamma t + ik_z z)$, the dispersion relation for the growth rate becomes $\gamma = k_z \sqrt{\eta_{yx}(-q\Omega + \eta_{xy}k_z^2)} - \eta_t k_z^2$. In the limit where $|q\Omega| \gg \eta_{xy}k_z^2$, this simplifies to $\gamma \simeq k_z \sqrt{-q\Omega\eta_{yx}} - \eta_t k_z^2$. This form highlights that a negative η_{yx} drives the exponential growth of the large-scale magnetic field, while η_t represents the net damping effect from all dissipative processes.

S2: Pressure Fluctuations

We now analyze the contributions from gas and magnetic pressure fluctuations, and their effect on the mean EMF that drives large-scale radial magnetic fields. The pressure fluctuations become significant in the vertical component of the fluctuating Lorentz force, particularly in the evolution of u_z , which contributes to the EMFs through $\bar{F}_{zx} = \langle u_z b_x \rangle$ and $\bar{F}_{zy} = \langle u_z b_y \rangle$. Instead of detailing each term in the evolution equations for \bar{F}_{zx} and \bar{F}_{zy} , we focus on the contributions from gas ($\bar{\mathcal{P}}_y^g$) and magnetic ($\bar{\mathcal{P}}_y^b$) pressure fluctuations, where $(\bar{\mathcal{P}}_y = \bar{\mathcal{P}}_y^g + \bar{\mathcal{P}}_y^b)$, as they appear in $\bar{\mathcal{E}}_y$ (Eq. 3) and contribute to the evolution of \bar{B}_x (Eq. 4), which is the primary focus of this study. The magnetic pressure fluctuations, given

by $p_b = (b^2 + 2\bar{B} \cdot b - \bar{b}^2)/2\mu_0$, yield

$$\begin{aligned} \bar{\mathcal{P}}_y^b &= \frac{-1}{q(2-q)\rho\Omega} \left[(2-q) \{ \bar{M}_{yy} \partial_z \bar{B}_y + \bar{M}_{xy} \partial_z \bar{B}_x \} \right. \\ &\quad + \bar{B}_k \left\{ -q \frac{\langle b_z \partial_y b_k \rangle}{\mu_0} + (2-q) \frac{\langle b_y \partial_z b_k \rangle}{\mu_0} \right\} \\ &\quad + \left. \left\{ -q \frac{\langle b_z \partial_y b^2 \rangle}{2\mu_0} + (2-q) \frac{\langle b_y \partial_z b^2 \rangle}{2\mu_0} \right\} \right], \\ &= \alpha_{yj}^p \bar{B}_j + \beta_{yyz}^p \partial_z \bar{B}_y + \beta_{yxz}^p \partial_z \bar{B}_x + \bar{\mathcal{T}}_y^p, \end{aligned} \quad (\text{S4a})$$

$$\bar{\mathcal{P}}_y^g = \frac{-1}{q(2-q)\rho\Omega} \left\{ -q \langle b_z \partial_y p_g \rangle + (2-q) \langle b_y \partial_z p_g \rangle \right\}. \quad (\text{S4b})$$

Magnetic pressure fluctuations contribute to the EMF through turbulent diffusivity tensors η_{ij} , α_{ij} tensors, and third-order correlators. A crucial aspect is the negative

η_{ij} tensors, which can drive dynamo action, given by

$$\eta_{yx}^p = \beta_{yyz}^p = -\frac{1}{\rho q \Omega} \bar{M}_{yy}; \quad \eta_{yy}^p = -\beta_{yxz}^p = \frac{1}{\rho q \Omega} \bar{M}_{xy}. \quad (\text{S5})$$

In MRI turbulence, \bar{M}_{xy} is consistently negative, while \bar{M}_{yy} remains positive. Consequently, both η_{yx}^p and η_{yy}^p are negative, serving as source terms for \bar{B}_x generation. Previous studies on shear-flow turbulence reported negative η_{yy} , though without a detailed explanation, often deeming it unphysical [25, 34, 38]. Here, we demonstrate that the negative η_{yy} arises from magnetic pressure fluctuations via the correlator \bar{M}_{xy} , which is responsible for outward angular momentum transport in accretion disks. Despite their dynamo role, the contributions of magnetic pressure fluctuations are largely canceled by those from gas pressure fluctuations, resulting in a negligible net effect. These findings are illustrated in Fig. S1, which presents the contributions of gas and magnetic pressure fluctuations to $\bar{\mathcal{E}}_y$ during the exponential growth phase of MRI at $t/T_{\text{orb}} = 3.34$. The total contribution of these fluctuations ($\bar{\mathcal{P}}_y$) is shown in Fig. 1(a), while individual contributions from four distinct components of magnetic pressure fluctuations are displayed in the bottom legend.

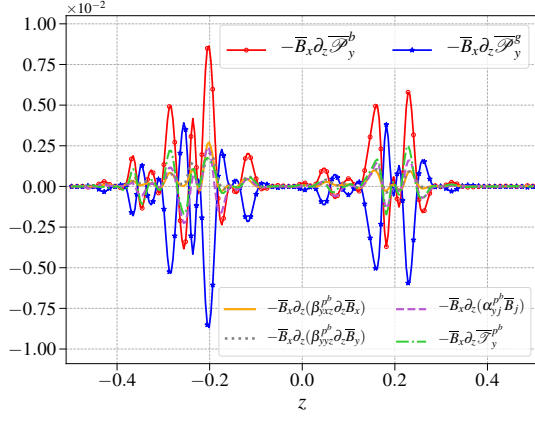


FIG. S1: Spatial variation of terms associated with magnetic (Eq. S4a) and gas pressure fluctuations (Eq. S4b) contributing to \bar{B}_x evolution via $\bar{\mathcal{E}}_y$ (Eq. 4) during the exponential growth phase of MRI, evaluated at $t/T_{\text{orb}} = 3.34$. The total effect of these fluctuations ($\bar{\mathcal{P}}_y$) is shown in Fig. 1(a), while individual contributions from four components of magnetic pressure fluctuations (Eq. S4a) are displayed in the bottom legends.